A Three-Phase Bidirectional Variable Speed Drive: An Experimental Validation for a Three-Phase Induction Motor

Luis Machado, Tiago J. C. Sousa, Delfim Pedrosa, Vitor Monteiro[✉], J. G. Pinto, and Joao L. Afonso

Centro ALGORITMI, University of Minho, Campus de Azurém, Guimarães, Portugal
{lmachado,vmonteiro}@dei.uminho.pt

Abstract. This paper presents the implementation and subsequent experimental verification of an electronic variable speed drive (VSD) for driving an induction motor, which is composed by a three-phase ac-dc converter on the grid-side and by a three-phase dc-ac converter on the motor-side. With the proposed solution, besides driving the motor, it is possible to mitigate power quality problems on the grid-side (e.g., current harmonics and power factor) associated with the use of diode-bridge ac-dc converters in the conventional VSDs. Besides, with the proposed solution, a bidirectional operation is possible, allowing to deliver to the power grid the energy generated in motor braking processes. As demonstrated along the paper, with the proposed VSD, it is possible to control the motor speed (including the rotation direction), and the operation with sinusoidal currents and unitary power factor on the grid-side. A laboratory prototype was developed, permitting to perform an experimental validation and prove the main functionalities of the VSD.

Keywords: Variable speed drive · Active rectifier · Induction motor · Regenerative braking · Power quality

1 Introduction

Nowadays, the three-phase induction motor with squirrel cage rotor represents more than 90% of the electric motors used in industry, contributing to more than 60% of industrial electricity consumption. This situation occurs, not only because the induction motors present low acquisition and maintenance costs and great robustness, but mainly due to constant technological evolution and the development of control techniques that have brought a wider variety of applications [1–3].

Conventionally, variable speed drives (VSDs) for induction motors employ a diode bridge rectifier in order to provide power to the dc-link from the power grid. Although this type of rectifiers is an economical solution, they contribute to the degradation of power quality, since they consume currents with high harmonic content that, in turn, cause distortions in the voltage waveform and low power factor amount of the VSD. Besides,

they do not allow reversing the energy flow, thus rendering the regenerative braking process to the power grid impracticable. For power quality improvement, passive or active filters are frequently installed, meaning additional investment costs [4]. A more recent solution consists in used active rectifiers [4]. Thus, the passive ac-dc converters have been replaced by active ac-dc converters, which present the following advantages as attractive [5, 6]: regulated voltage supply with low ripple to the dc-link; sinusoidal current consumption; maximization of the power factor; and bidirectional power flow, which allows an effective use of the electrical energy generated in braking or decelerating situations of the motor, returning it to the power grid instead of being dissipated in a resistor (braking resistor), or stored in storage elements such as ultracapacitors or batteries [7].

Significant technological advances have emerged in the field of VSDs over the last few years [1]. This growth has been felt in the market of electric motors, especially as regards the sale of induction motors, which has increased, and it is thought that it will continue to increase, not only because of the qualities they have in relation to the dc motors very used in the past, but mainly because of the evolution of VSDs, which has allowed the use of these motors in variable speed applications [1].

The paper is structured as follows: Sect. 2 presents the electrical model of the proposed system under analysis; Sect. 3 presents the implemented control algorithm for each of the power converters; Sect. 4 presents the developed prototype and the obtained experimental results of the VSD and Sect. 5 finalizes the paper with the conclusions.

2 Proposed System

This section presents the electrical model of the proposed system under analysis in this paper. As previously mentioned, a typical topology of a VSD for three-phase induction motors, usually, has a diode bridge rectifier for interfacing with the power grid, also known in the literature as a Graetz bridge [8]. As a disadvantage, this type of converter does not control the input (nor the output) current nor the dc-link voltage (v_{dc}), which is limited to the peak value of the power grid phase voltages. In this way, the proposed system suggests the exchange of the passive semiconductors by active semiconductors, resulting in the electric model of Fig. 1. In this figure, two voltage source converters (active rectifier and inverter) can be seen, both with three legs with two insulate gate bipolar transistors (IGBTs) in each leg. The fact that this topology has only three wires allows to simplify the solution and reduce the costs related with the addition of a fourth IGBT leg for the neutral connection or, if it is connected to the midpoint of the dc-link capacitors, reduce the complexity associated with the voltage regulation in each capacitor terminals.

The converters are connected through a dc-link consisting of a capacitive filter (C_{dc}), whose function is to minimize the ripple of the v_{dc} voltage. At the input of the active rectifier, coupling inductors (L_a, L_b, L_c) are used to smooth the absorbed currents (i_a, i_b, i_c). The stator windings of the induction motor were used to smooth the currents at the output of the inverter (i_{am}, i_{bm}, i_{cm}).
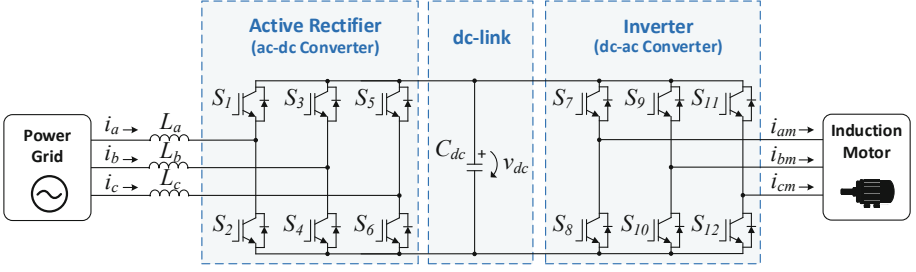
Fig. 1. Proposed system for the VSD.

3 Control Algorithm

This section presents the control algorithm implemented for the proposed solution. For a better understanding, it is divided into two parts: control for the active rectifier and control for the traction system, which involves the inverter and motor.

3.1 Active Rectifier

The block diagram of the strategy used to control the active rectifier can be seen in Fig. 2. In this control strategy, the dc-link voltage (v_{dc}) is measured and compared to the reference value (v_{dc_ref}), from where results the error signal v_{dc_er}, which is submitted to a proportional-integral controller (PI). Posteriorly, the output of this controller is multiplied by each of the sinusoidal references (pll_a, pll_b, pll_c) with unitary amplitude and frequency and phase equal to the fundamental component of the respective power grid voltage. These references are obtained from the ωt angle resulting from the phase locked-loop (PLL) based on the p-q theory [9–13], corresponding to three sinusoidal signals with phase synchronized with the phase of power grid voltage and amplitude i_{pk_ref} dependent of the error and the gains of the PI controller. The currents i_{a_ref}, i_{b_ref} and i_{c_ref} are the reference currents for each input currents (i_a, i_b, i_c). The reference voltages are calculated using a predictive control technique [14–17], which is represented by (1), where ref_x refers to the reference voltage that the converter must produce in phase x, which is calculated based on the simple power grid voltage (v_x), the coupling inductance value per phase (L_x), the sampling time (T_s), the phase current measured at the input of the rectifier (i_x), its reference current (i_{x_ref}) and the current measured at the previous instant ($i_{x\_ref\_pr}$). It should be noted that the voltage drop in the inductor resistive component was not used, since its value can be neglected when compared to the voltage drop in the inductive component.

$$ref_x = v_x - \frac{L_x}{T_s}\left[2i_{x\_ref} - i_{x\_ref\_pr} - i_x\right] \tag{1}$$

From the reference signals, in order to generate the appropriate duty-cycle of the pulses to be applied to the gates of the IGBTs, the sinusoidal pulse-width modulation (SPWM) method was used.
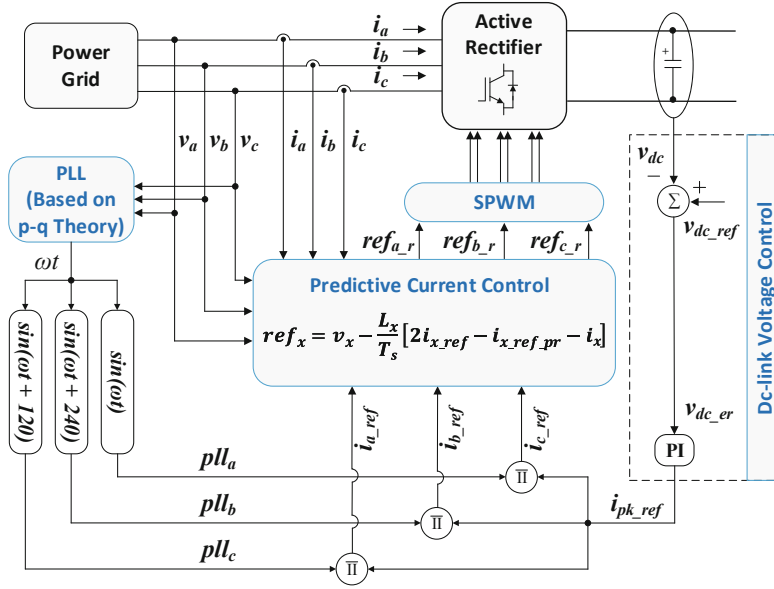
Fig. 2. Control diagram for the rectifier stage of the VSD.

3.2 Motor Control

For the motor control, the closed loop *Volts per Hertz* control was chosen [18–21]. Compared to vector control techniques, it is simpler, more economical and easier to implement [18–21], and is recommended for non-critical applications where good speed and/or torque performances are not relevant [3].

Figure 3 shows the designed block diagram of the control loop implementation for the traction system. As it can be seen, the rotor speed, ω_r, is compared with the reference speed ω_{r_ref} from where, by application of a PI controller, a signal (ω_d) is obtained, which has to be added to the rotor speed in order to obtain the desired synchronous speed (ω_{s_ref}). Once calculated ω_{s_ref}, and, based on this, calculated f_{s_ref} through a pre-established *V/f* ramp, the respective voltage amplitude (v_{s_ref}) that must be applied to each of the stator windings is obtained by (2). A low-frequency compensation part, an offset voltage V_0, should be included in the voltage/frequency relation.

$$V_{s\_ref} = \frac{V_s}{f_{nom}} f_{s\_ref} + V_0 \tag{2}$$

On the other hand, the integration of ω_{s_ref} results in the signal θ_{ref} that defines the frequency of the reference voltages, obtain by (3), that must be synthesized and subsequently applied to a modulation technique. As in the control of the active rectifier, the modulation technique used in the inverter control was SPWM.

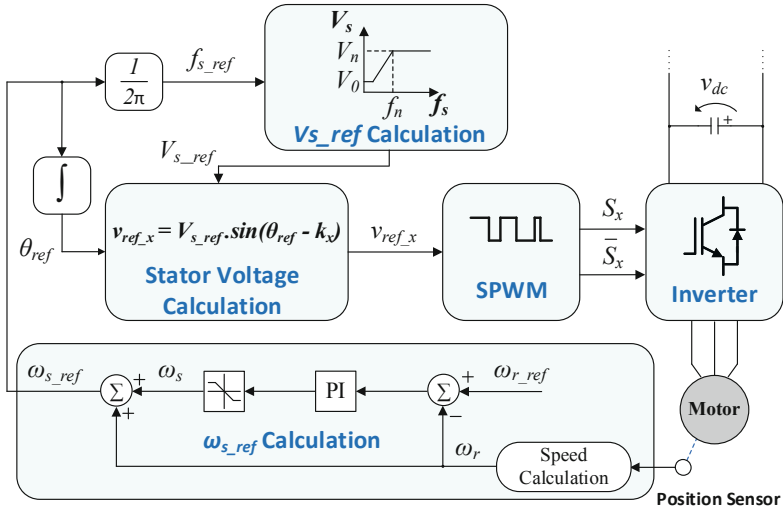$$v_{ref\_x} = V_{s\_ref} sin(\theta_{ref} - k_x) \tag{3}$$

Fig. 3. Control diagram for the inverter stage of the VSD.

4 Experimental Setup and Results

This section presents the obtained experimental results of the developed VSD prototype, which is shown in Fig. 4. At the top of the prototype, the two power converters can be seen, implemented with six SKM400GB12V half-bridge IGBT modules from Semikron.
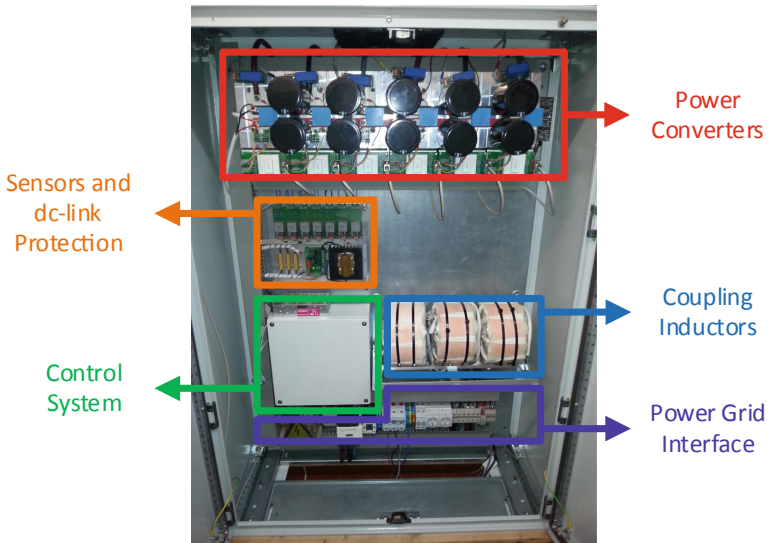

Fig. 4. Laboratory prototype of the developed VSD.

Each half-bridge are driven by a SKHI22AR driver, also from Semikron. For all IGBTs, a 5 kHz switching frequency is used.

The dc-link, also at the top, is built by a set of capacitors with a total capacitance of 5.5 mF and a maximum voltage of 900 V. Immediately below of the power converters, can be seen the sensors used to measure the system variables, as well as the dc-link protections for overvoltages above 900 V. Further down, on the left, it can be seen the control system platform, based on a TMS320F28335 DSP of Texas Instruments, and, on the right, can be found the coupling inductors for the active rectifier. At the bottom of the prototype stands all the necessary logic for the pre-charger system of the dc-link capacitors and the prototype interface with the power grid.
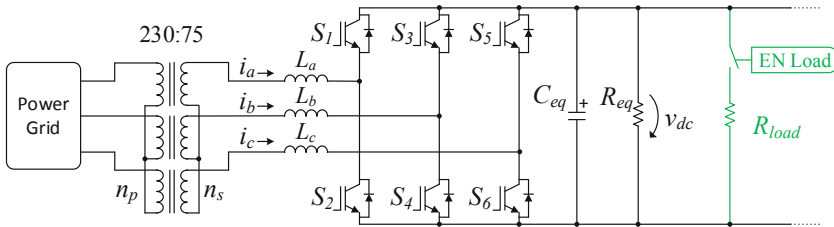

Fig. 5. Power circuit used to obtain the experimental results of the VSD active rectifier.

4.1 Active Rectifier Results

The experimental results concerning the operation of the active rectifier were obtained based on the scheme of Fig. 5. As it can be seen, the power grid voltage is reduced from root mean square (rms) value of 230 V to 75 V by using a group of three single-phase star-connected transformers. In the dc-link, a resistive load (R_{load}) of 25 Ω was placed in series with a circuit breaker, it can be connected or disconnected from the dc-link at certain moment. With this, it was intended to validate the control of the dc-link voltage and simultaneously the predictive current control. The inductance value (L_a, L_b, L_c) of each coupling inductor, the equivalent capacitance value (C_{eq}) and the equivalent equalization resistance (R_{eq}) of the dc-link are, respectively, 3.5 mH, 5.5 mF and 8.4 kΩ.

With the dc-link voltage regulated at 250 V, at a certain moment, the load of 25 Ω was connected (Fig. 6(a)), with an expected drop in dc-link voltage. In steady state, the grid currents (i_a, i_b, i_c) were obtained in the three phases with amplitude of 17 A, in phase with the respective phase-neutral power grid voltages (v_a, v_b, v_c) (Fig. 6(b)). These currents have a total harmonic distortion (THD) in relation to the fundamental component of 1.6%, 1.4% and 1.7% for phases a, b and c, respectively.

In order to validate the operation of the ac-dc converter as an inverter, a dc-link voltage of 120 V was fixed with a voltage source. Due to the modulation index used (85%) and to the available voltage sources, it was necessary to reduce to the power grid voltage, having been changed to 25 V rms. Results were obtained for peak currents reference of 1 A (Fig. 7(a)) and 2 A (Fig. 7(b)). With these results, it was verified that the harmonic distortion of the currents injected into the power grid is greater when the amplitude of the currents is smaller, which is expected, considering that the signal-to-noise ratio is lower in this case.
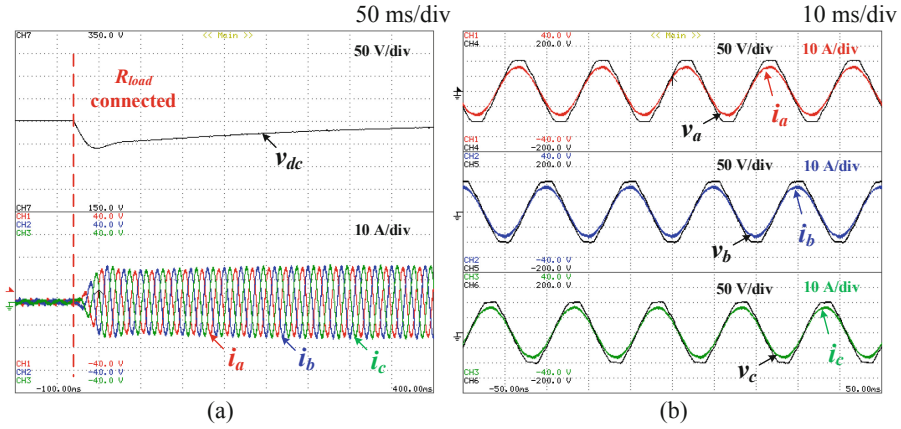
Fig. 6. Active rectifier operation with a 25 Ω load connected to the dc-link: (a) Transient state dc-link voltage and power grid currents; (b) Steady state power grid voltages and currents.
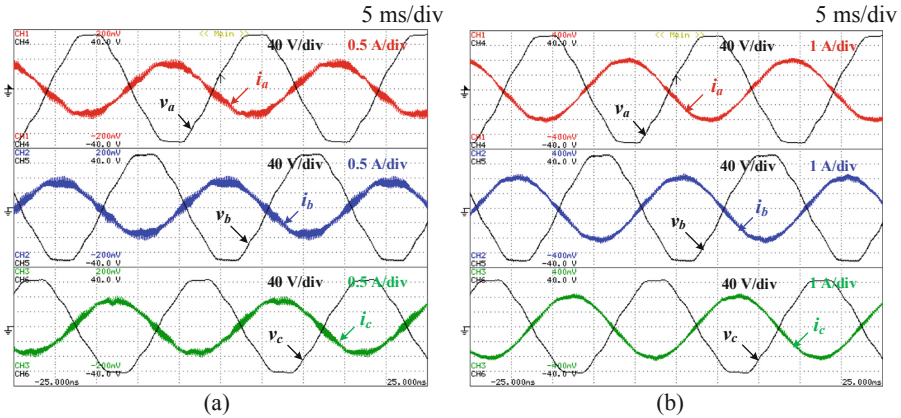

Fig. 7. Power grid voltages and currents for the active rectifier operation for a peak current of: (a) 1 A; (b) 2 A.
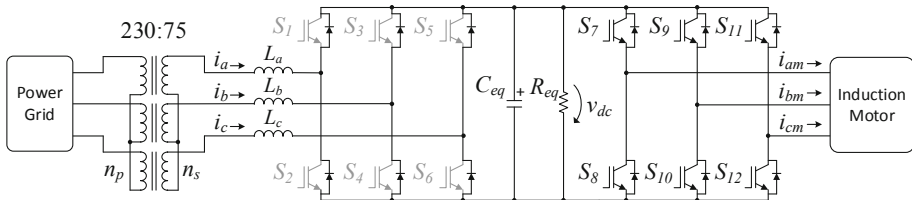

Fig. 8. Power circuit used to obtain the experimental results to VSD.

4.2 Motor Control Results

The experimental results for the motor control were obtained with a 5.5 kW induction motor with nominal speed of 920 rpm, 3 pole pairs, voltage, current and nominal torque of 380 V, 12.3 A and 57.1 Nm, respectively.

In order to carry out the experimental tests, the dc-link was, in a first moment, fed from the power grid through the diodes of each of the fully controllable semiconductors of the rectifier stage (Fig. 8). Thus, the grid voltage (75 V rms) was rectified, resulting in a dc-link voltage close to the peak value of the phase-to-phase voltages, which is slightly lower due to voltage drops in the coupling inductors, voltage drops on the diodes of the converter and also due to the equivalent resistance value of 8.4 kΩ on the dc-link which, although not properly low, is not negligible. It is important to note that the results were only possible to obtain because it was assumed a voltage V_s (present in Eq. (2)) applied to the stator equal to the maximum voltage produced by the converter instead of considering the motor nominal voltage.

In the first test, the induction motor was subjected to a constant load of 3 Nm at different reference speed values (n_{ref}) and the experimental result of Fig. 9(a) was obtained. As it can be seen, initially, the motor was rotating with a speed (n) of 200 rpm in a given direction. After about 1 s the direction of rotation was reversed. At this instant, as the figure shows, the reversal voltage braking was given until the speed is annulled, and the dc-link voltage was slightly increased. From this speed (0 rpm), the motor accelerated until reaching the reference speed of 200 rpm, which took place after 2 s. During this acceleration, as a consequence of the consumed currents (i_{am}, i_{bm}, i_{cm}) (about 15 A peak), the appearance of a sag of approximately 23 V in the dc-link voltage is notorious.

Then, the behavior of the motor with an applied load torque of 5 Nm was tested also for different rotation speeds. The result obtained is shown in Fig. 9(b). During the first two seconds, an oscillation of the motor rotation speed is visible around the reference speed of 400 rpm. This oscillation tends to decrease as the speed decreases, as it can be seen.

During the speed changes, it is possible to observe the charging of the dc-link capacitors, with a maximum voltage on the dc-link close to 240 V at the transition from 400 rpm to 350 rpm. Since in these tests a diode bridge rectifier was used, the current cannot flow to the power grid, so the energy generated by the motor during braking is stored in the dc-link capacitors.

Posteriorly, the ac-dc converter was placed to function as the active rectifier. At this stage a load torque of 5 Nm was applied to the motor shaft, and this was carried out at a rotational speed of 600 rpm, which, after some time, was increased to 800 rpm. After that, the results of Fig. 10(a) are presented, where the current absorbed in phase a (i_a) and the respective phase neutral power grid voltage (v_a) are shown. As can be seen, the current is in phase with the power grid voltage. It is also possible to see that the distortion of the current at the input of the rectifier (i_a) tends to decrease with the increase of the current, as previously verified in the results obtained for the operation of the ac-dc converter as inverter.

Then, in order to analyze the behavior of the system in the event of motor deceleration, the speed of 800 rpm was reduced again to 600 rpm and the results of Fig. 10(b) were obtained. As it can be seen, the current at the input of the rectifier in phase a (i_a) has
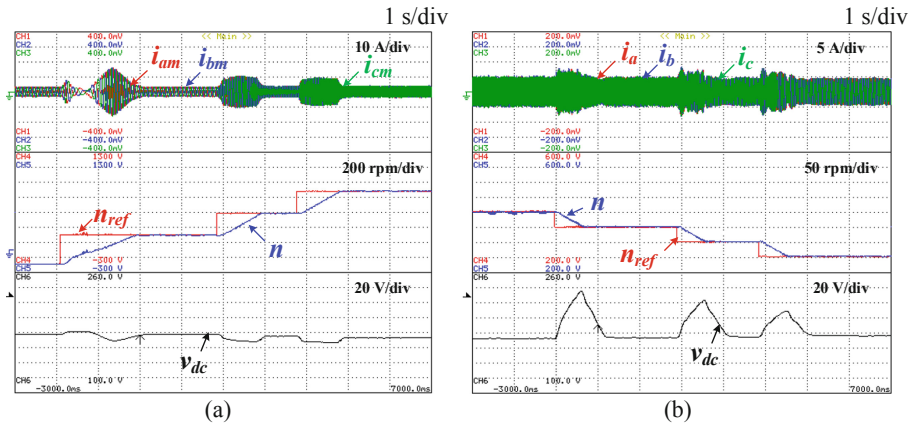
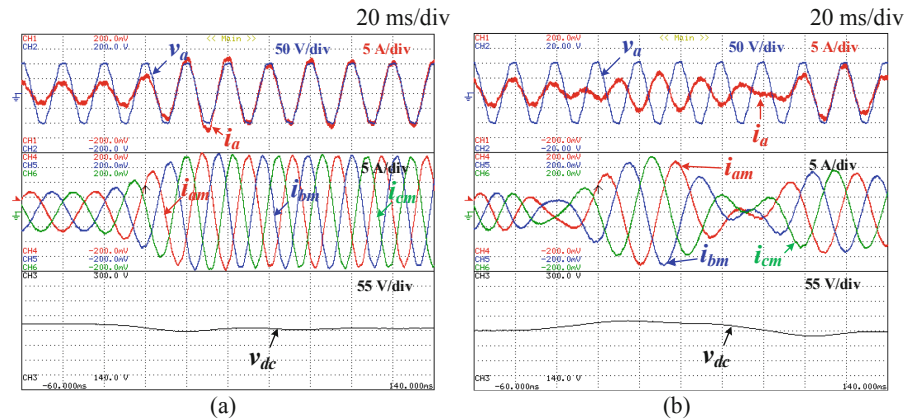**Fig. 9.** Results obtained in the operation of the motor for a constant load of: (a) 3 Nm; (b) 5 Nm.

Fig. 10. Results obtained for the motor driving a 5 Nm load during: (a) Acceleration from 600 rpm to 800 rpm; (b) Deceleration from 800 rpm to 600 rpm.

become in phase opposition with the voltage v_a, remaining in this situation for about four power grid cycles. During this time, the current was injected into the power grid, therefore the ac-dc converter was used as an inverter. Also, for this situation, there was an increase of the dc-link voltage by about 14% of the voltage set for regulation (250 V).

5   Conclusions

This paper presents an analysis of a variable speed drive (VSD), which makes use of a three-phase ac-dc power converter to interface with the power grid, and a three-phase dc-ac converter to drive a three-phase induction motor, both converters sharing a capacitive dc-link. An electrical model of the system was developed and, based on it, a laboratory prototype was developed, from which the experimental results presented in this paper

were obtained. These results achieved the objective concerning the experimental validation of the proposed control algorithms, specifically predictive current control (active rectifier) and closed loop *Volts per Hertz* control (motor speed control). Thus, it was possible to verify the capability of the system to compensate power quality problems, in particular, in relation to the currents consumed on the grid side, which presented sinusoidal waveforms, low harmonic content and unitary power factor. In relation to the motor control, its operation was validated in the traction mode, as well as in the braking mode, returning the generated energy to the power grid (regenerative braking).

References

1. Almeida, A., Fong, J., Falkner, H., Bertoldi, P.: Policy options to promote energy efficient electric motors and drives in the EU. Renew. Sustain. Energy Rev. **74**, 1275–1286 (2017)
2. Chavhan, K., Ugale, R.: Automated test bench for an induction motor using LabVIEW. In: IEEE International Conference on Power Electronics, Intelligent Control and Energy Systems (ICPEICES), pp. 1–6, July 2016
3. Alsofyani, I., Idris, N.: A review on sensorless techniques for sustainable reliablity and efficient variable frequency drives of induction motors. Renew. Sustain. Energy Rev. **24**, 111–121 (2013)
4. Michalik, J., Smidl, V., Peroutka, Z.: Control approaches of current-source rectifier: predictive control versus PWM-based linear control. In: IEEE International Conference on Power Electronics and Drive Systems (PEDS), December 2017
5. Begag, S., Belhaouchet, N., Rahmani, L.: Three-phase PWM rectifier with constant switching frequency. J. Electr. Syst. **5**(1), 7–12 (2009)
6. Cho, J., Jeong, C., Baek, J., Song, D., Yoo, D., Won, C.: High power factor three phase rectifier for high power density AC/DC conversion applications. In: Applied Power Electronics Conference and Exposition, vol. 2, pp. 910–915, March 1999
7. Ekstrom, A., Liss, G.: A refined HVDC control system. IEEE Trans. Power App. Syst. **PAS-89**(5), 723–732 (1970)
8. Saidur, R., Mekhilef, S., Ali, M., Safari, A., Mohammed, H.: Applications of variable speed drive (VSD) in electrical motors energy savings. Renew. Sustain. Energy Rev. **16**, 543–550 (2011)
9. Rolim, L., da Costa, D., Aredes, M.: Analysis and software implementation of a robust synchronizing PLL circuit based on the pq theory. IEEE Trans. Industr. Electron. **53**(6), 1919–1926 (2006)
10. Thacker, T., Boroyevich, D., Burgos, R., Wang, F.: Phase-locked loop noise reduction via phase detector implementation for single-phase systems. IEEE Trans. Industr. Electron. **58**(6), 2482–2490 (2011)
11. Golestan, S., Monfared, M., Freijedo, F., Guerrero, J.: Design and tuning of a modified power-based PLL for single-phase grid-connected power conditioning systems. IEEE Trans. Power Electron. **27**(8), 3639–3650 (2012)
12. Golestan, S., Guerrero, J., Vasquez, J.: Three-phase PLLs: a review of recent advances. IEEE Trans. Power Electron. **32**(3), 1894–1907 (2017)

13. Guo, X., Wu, W., Gu, H.: Phase locked loop and synchronization methods for grid-interfaced converters: a review. Przeglad Elektrotechniczny **87**(4), 182–187 (2011)
14. Bosch, S., Staiger, J., Steinhart, H.: Predictive current control for an active power filter with LCL-filter. IEEE Trans. Industr. Electron. **65**, 4943–4952 (2017)
15. Pinto, J.: Nova Topologia de UPQC sem Transformador para Compensação de Problemas de Qualidade de Energia Elétrica. Doctoral thesis, University of Minho, Guimarães (2011)
16. Kumar, K., Michael, P., John, J., Kumar, S.: Simulation and comparison of SPWM and SVPWM control for three phase inverter. ARPN J. Eng. Appl. Sci. **5**(7), 61–74 (2010)
17. Bacon, V., Campanhol, L., Silva, S.: Análise Comparativa das Técnicas SPWM e SVM Aplicadas a um Inversor de Tensão Trifásico. UNOPAR Científica Ciências Exatas e Tecnológicas **10**(1) (2015). http://www.pgsskroton.com.br/seer/index.php/exatas/article/view/508/479. Accessed 28 May 2017
18. Tembhekar, K.: Improvement and analysis of speed control of three phase induction motor drive including two methods. In: 2nd International Conference on Emerging Trends in Engineering and Technology (ICETET), pp. 736–741 (2009)
19. Ross, D., Theys, J., Bowling, S.: Using the dsPIC30F for vector control of an ACIM. Microchip Technologies (2004). http://ww1.microchip.com/downloads/jp/AppNotes/ACIM%20Vector%20Control%2000908a.pdf. Accessed 15 Sept 2017
20. Bodkhe, S., Aware, M.: A variable-speed, sensorless, induction motor drive using DC-link measurements. In: 4th IEEE Conference on Industrial Electronics and Applications, pp. 3591–3596, June 2009
21. Habbi, H.M.D., Ajeel, H.J., Ali, I.I.: Speed control of induction motor using PI and V/F scalar vector controllers. Int. J. Comput. Appl. **151**(7), 36–43 (2016)